

Mechanochemistry of shock-induced nanobubble collapse near silica in water

K. Nomura,¹ R. K. Kalia,¹ A. Nakano,¹ P. Vashishta,¹ and A. C. T. van Duin²

¹*Collaboratory for Advanced Computing and Simulations, University of Southern California, Los Angeles, California 90089-0242, USA*

²*Department of Mechanical and Nuclear Engineering, Pennsylvania State University, University Park, Pennsylvania 16802, USA*

(Received 21 May 2012; accepted 31 July 2012; published online 14 August 2012)

We have performed million-atom reactive molecular dynamics simulations to study shock-induced bubble collapse near an amorphous silica surface. We observe the formation of water jet during the bubble collapse, which collides on to the silica surface causing a hemispherical pit. Fragment analysis reveals substantial ionization activities in water followed by rapid increase in H_3O^+ population during the pit formation. We have identified a shock-induced H_3O^+ ion formation mechanism, in which transient five-coordinated silicon atoms play a pivotal role. © 2012 American Institute of Physics. [<http://dx.doi.org/10.1063/1.4746270>]

Cavitation can be found in many engineering applications, for example, ultrasound cleaning takes advantage of cavitation bubbles to remove unwanted substance from material surfaces. Cavitation bubbles also often result in undesirable effects such as cavitation-mediated damage to pumps, propellers, and tissues surrounding kidney stone in shock wave lithotripsy.^{1,2} Recently, ultrasound has been attracting much attention as a surface modification technique³ since cavitation activity locally induces elevated-temperature and pressure at even ambient condition. An example is modifying the functionality of ceramics surface. Ceramics are generally hard, brittle, and chemically inert materials, however they are often susceptible to cavitation erosion. Niebuhr⁴ examined the cavitation performance of several engineering ceramics (Al_2O_3 , Si_3N_4 , glass-mica, and ZrO_2) in various media. Viro *et al.* used a power ultrasound technique to investigate an interface between water and silica glass.⁵ They have found that bubble collapse at the glass-water interface is an important factor not only to initiate mechanical erosion but also enhance material leaching. These experiments have demonstrated that chemical composition, microstructure, and aqueous media largely affect their cavitation properties such as incubation time and weight loss. However, fundamental knowledge of cavitation erosion is still lacking, which prohibits desired control and design of surface functionality.

In the past decade, many experiments and continuum simulations have examined the collapse of bubbles near a rigid boundary and also in the vicinity of an elastic membrane.^{2,6} In particular, high-speed photography experiments on a single laser-generated bubble have provided considerable insight into the dynamics of collapse. The dynamics has been comprehensively mapped out as a function of the dimensionless standoff parameter $g = d/R_m$, where d is the separation between the center of the bubble and the rigid surface and R_m is the maximum radius of the bubble. It is observed that the bubble collapse generates a high-speed liquid jet, which can cause significant damage to the rigid body. Cavitation damage on a rigid surface appears in the form of a shallow pit or a circular pattern. Pitting is a serious techno-

logical problem because residual stresses at a pit can cause stress corrosion cracking of materials.

An interesting aspect that neither experiments nor simulations have yet examined is the mechanochemistry of cavitation bubble collapse in water near a rigid boundary or an elastic membrane. It is well known that water molecules in the liquid phase dissociate into hydronium (H_3O^+) and hydroxide (OH^-) ions. These autoionization events in liquid water are rare, occurring at the molecular scale once in approximately 10 h.^{7,8} This naturally raises the question: Does the collapse of a cavitation bubble enhance autoionization in liquid water, especially near a solid boundary? A second, related question is: Does the impact of high-velocity liquid jets induce significant structural and chemical changes in the solid?

In this letter, we examine these chemical and mechanical aspects⁹ of shock-induced nanobubble collapse near an archetypal ceramic, amorphous silica, using molecular dynamics (MD) simulations based on a reactive force field (ReaxFF).^{10,11} The first principles-based ReaxFF (Ref. 12) allows bond breaking and bond formation through reactive bond orders^{13,14} and dynamical charges by employing an electronegativity-equalization scheme.¹⁵ The initial setup of the system involved two sets of MD simulations in the microcanonical ensemble (1) to equilibrate a system of 368 640 water molecules in an MD cell of dimensions $35.81 \times 18.61 \times 16.60 \text{ nm}^3$ at room temperature and (2) to prepare bulk amorphous silica (a-SiO₂) at room temperature with the melt-quench method. Periodic boundary conditions (PBCs) were imposed in both cases. Next, we removed water molecules in the first system to embed a slab of a-SiO₂ cut out of bulk a-SiO₂. All undercoordinated atoms introduced by the cut are terminated with hydrogen atoms and OH groups to avoid the breaking of water molecule. The slab thickness is 5.3 nm and it contains 97 650 atoms, including the terminating hydrogen atoms on the slab surface. The slab is located between $x = 23.5 \text{ nm}$ and $x = 28.8 \text{ nm}$. Subsequently, we created a nanobubble by removing water molecules from a spherical region of radius 5 nm centered at $x = 12.7 \text{ nm}$, $y = 9.3 \text{ nm}$, and $z = 8.3 \text{ nm}$. To model shock waves and

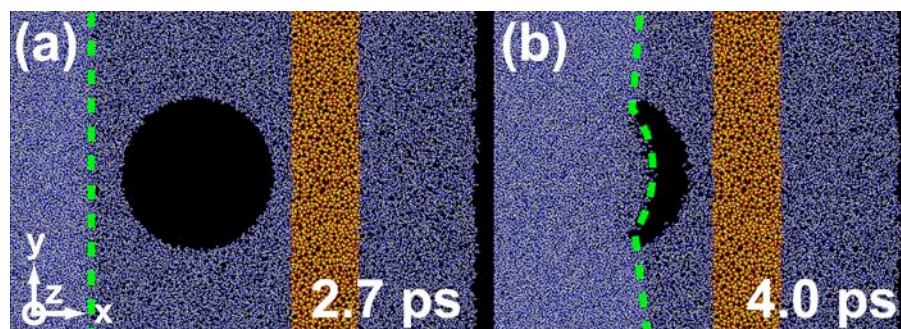


FIG. 1. (a) A snapshot ($t = 2.7$ ps) of a planar shock wave (green-dotted line indicates the shock front), a spherical nanobubble (black), and the silica slab (orange) embedded in water (blue). For clarity, only 1 nm thick slice at the middle of the system is shown. (b) At $t = 4.0$ ps, the nanobubble has partially collapsed and a high-speed nanojet is formed as water molecules rush into the nanobubble.

subsequent bubble collapse observed in experiments,¹⁶ we employ a planar shock wave using a momentum mirror technique.^{17,18} To apply a planar shock, we assigned a uniform particle velocity u_p on the entire system—water, nanobubble, and slab—towards a momentum mirror (located at $x = 0$), which reverses an atom's velocity component normal to the mirror when it crosses the mirror plane. We use a time step of 0.1 fs in all simulations.

Figure 1(a) is a snapshot of a shock wave approaching a spherical nanobubble of radius 5 nm located at a distance of 1 nm from the proximal side of the silica slab. Here the velocity of the shock wave before it hits the nanobubble is 6.6 km/s. The shock wave impact shrinks the bubble and collapses it completely in 1.7 ps. From the Rayleigh formula, we estimate the bubble collapse time ($\tau \approx 0.45D\sqrt{\rho/\Delta P}$, where D is the diameter of the bubble, ρ is the mass density, and ΔP is the peak pressure in the shock wave) to be 1.4 ps. The simulation result for the collapse time differs from that given by the Rayleigh formula because the latter does not take into account the viscosity of the fluid or the surface tension of the bubble.

Furthermore, the Rayleigh formula is derived with the assumption that the bubble is within a uniform fluid, which is not the case when the shock front impacts the bubble. During the nanobubble collapse, water molecules flow into the bubble and form a nanojet (see Fig. 1(b)).

During the nanobubble shrinkage, water molecules rush towards the center of the bubble, becoming a narrowly focused beam. Figures 2(a) and 2(b) show velocity profiles of those water molecules at two instants of time, corresponding to partial and total collapse of the nanobubble, where the velocity vector field is represented by streamlines. From the onset of bubble shrinkage, we observe water molecules around the top and bottom of the nanobubble being pushed towards the center of the bubble in the form of a nanojet. The nanojet continues to grow even after the collapse of the nanobubble. We have performed several simulations with the same system setup but different bubble diameters $D = 6, 8,$ and 10 nm. Obtained tip length L_{jet} shows linear scaling $L_{\text{jet}} \cong 0.15D$, which is similar to the jets observed experimentally in the collapse of micron size bubbles.¹⁶

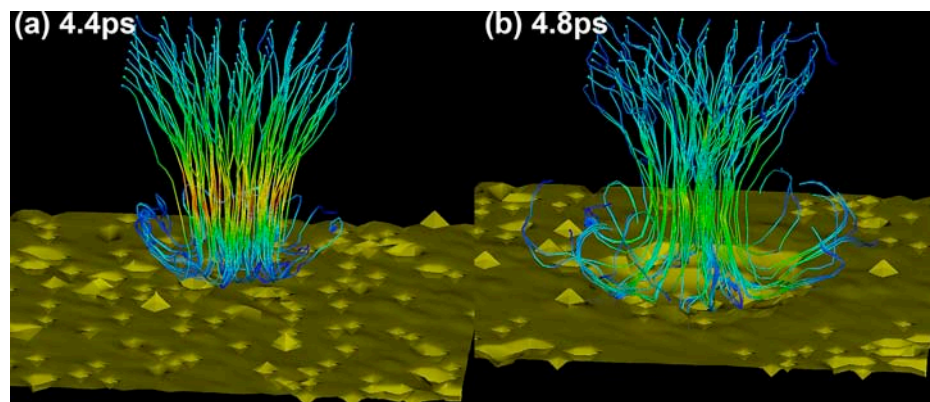


FIG. 2. Snapshots of flow patterns of water molecules during (a) and after (b) the nanobubble collapse. Streamlines are color-coded by the magnitude of averaged water molecule velocities. The surface of the silica slab proximal to the nanobubble is shown in yellow. In panel (a), water molecules flow into the nanobubble, creating a nanojet, which has bounced back by the silica slab. Panel (b) shows a hemispherical pit formation on the silica slab surface after the nanojet impact.

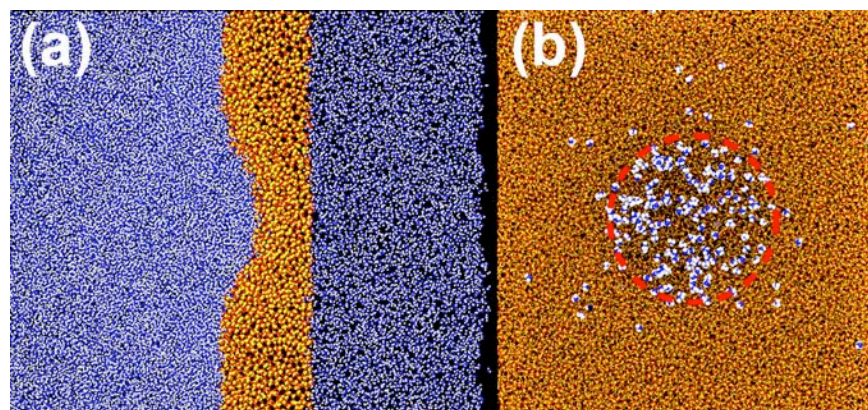


FIG. 3. (a) Snapshot after the pit formation ($t = 5$ ps) in the silica slab. After the shock passage, the nanobubble collapses completely, leaving a hemispherical pit on the surface. (b) A top view of the pit region superimposed with the spatial distribution of H_3O^+ ions. Blue and white spheres represent oxygen and hydrogen atoms, respectively. For clarity, only H_3O^+ ions and the silica slab are shown. Red-dotted circle indicates the extent of the pit. Most of H_3O^+ ions form around the pit surface.

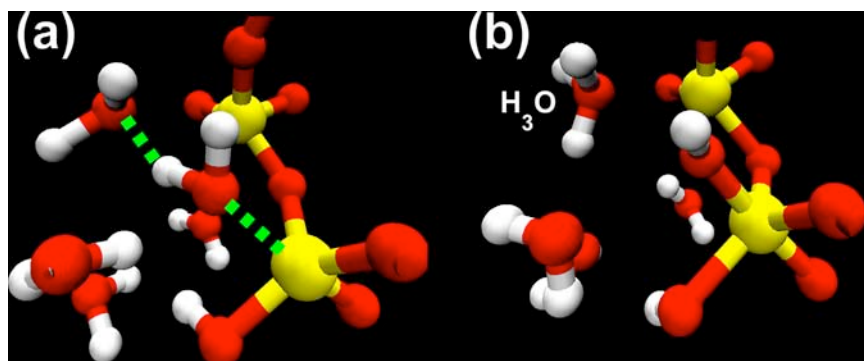


FIG. 4. Shock-induced H_3O^+ formation mechanism. Atomic configurations before (a) and after (b) the H_3O^+ formation are shown. White, red, and yellow spheres represent hydrogen, oxygen, and silicon atoms, respectively. In panel (a), green dotted lines indicate covalent bonds to be formed after the reaction (see panel (b)). One of the water molecules near the silicon atom splits into H^+ and OH^- ions. Shortly after, the OH^- ion transiently binds with the silicon atom, making it five-coordinated. The remaining H^+ ion binds with another H_2O molecule, becoming an H_3O^+ ion.

The simulations reveal significant ionization activity on the silica surface after the nanojet impact, which creates a hemispherical pit on the silica surface. Figure 3(a) shows a sideview of a 1 nm slice at the middle of the system after the nanojet impact ($t = 5$ ps). To quantify the ionization activity, we have performed fragment analysis, in which a cluster of covalently bonded atoms is considered as a chemical product.^{19,20} Note that before the nanojet impact, only H_2O molecules are found as a fragment besides a single large cluster for the silica slab. We found that H_3O^+ ion was the most prominent among all other chemical products. Also the formation of H_3O^+ ion is well localized near the pit surface. Figure 3(b) presents a top view near the pit region and the spatial distribution of H_3O^+ ions. It is noteworthy that the pit region contains not only hydronium and hydroxide ions but also silicic acid molecules and six-fold coordinated silicon atoms like those in the high-pressure stishovite phase of silica.²¹

Detailed analysis shows an atomistic mechanism for H_3O^+ ion formation mediated by a five-coordinated silicon atom on the slab surface. Figure 4(a) is an atomic configuration at the silica surface after the nanojet impact, showing

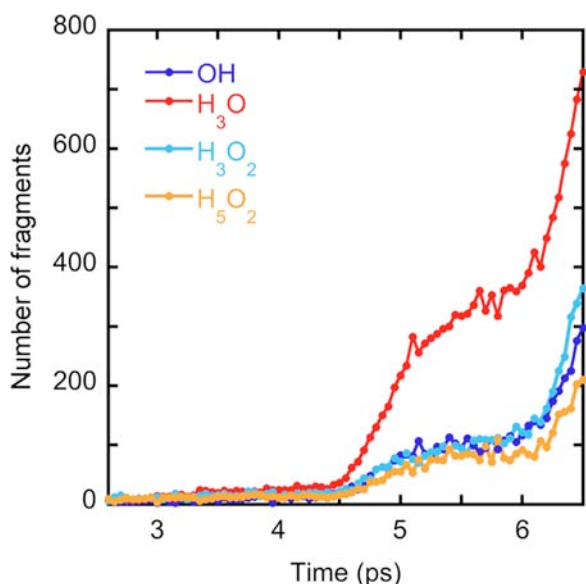


FIG. 5. Time evolutions of the population for OH^- , H_3O^+ , H_3O_2^- , and H_5O_2^+ ions. Although all ions show a similar trend, the H_3O^+ population is significantly greater than others. Around $t = 4.5$ ps, when the shock wave arrives at the slab surface, the ion populations increase rapidly. About $t = 5-6$ ps, when the shock propagating inside of the silica slab, the populations of ions do not change much. After $t = 6$ ps, the shock front starts interacting with the distal side of the slab surface resulting in the increase of the ion populations.

two H_2O molecules near one of SiO_4 units. The nanojet impact increases local pressure,^{17,18,22} which presses water molecules closer to the silica surface than in ambient condition. In Fig. 4(b), the water molecules near the SiO_4 unit dissociates into OH^- and H^+ . The OH^- ion transiently binds with the SiO_4 unit, making the silicon atom five-coordinated. At the same time, an H_3O^+ is produced from the remaining H^+ and the other H_2O molecule. Subsequently, the excess hydrogen transports in water by a chain of hydrogen-bond switching events, i.e., Grotthus mechanism.^{23,24}

To further characterize the ionization activity, Fig. 5 plots the number of molecular fragments in water as a function of time. Protonated water clusters have been studied as auto-ionization agents in bulk water.^{7,8,25} Here, we focus on the most noticeable four ions during the simulations, namely OH^- , H_3O^+ , H_3O_2^- , and H_5O_2^+ . After the nanojet impact at $t \sim 4.5$ ps, the H_3O^+ population shows a sharp increase compared to other ions, indicating H^+ release into water, leaving OH^- groups in the silica slab. During the shock propagation within the slab ($t = 5-6$ ps), the ion population becomes nearly constant. Subsequently, when the shock front has passed the distal side of the slab and the pit has maximally grown ($t > 6$ ps), the ion population starts increasing again.

In summary, we have performed million-atom ReaxFF MD simulations to study shock-induced bubble collapse near an amorphous silica surface. We observe the formation of water jet during the bubble collapse, which collides onto the slab surface creating a hemispherical pit. Simulations reveal that the collision between the water nanojet and the silica slab results in substantial ionization activities in water, mostly concentrated on the pit surface. Fragment analysis identifies the formation of a large number of H_3O^+ ions in water compared to other water-variant clusters. We have found a mechanically induced H_3O^+ generation mechanism on the amorphous silica surface, in which a silicon atom transiently becomes five-coordinated to split a water molecule into a silanol group and a hydronium ion in water.

This work was supported by DOE-SciDAC. Simulations were performed at the University of Southern California using the 20,925-processor Linux cluster at the High Performance Computing Facility, and at the Argonne Leadership Computing Facility using the 163,840-processor BlueGene/P computer under a DOE INCITE program.

¹C. E. Brennen, *Cavitation and Bubble Dynamics* (Oxford University Press, New York, 1995).

²E. Johnsen and T. Colonius, *J. Acoust. Soc. Am.* **124**(4), 2011–2020 (2008).

- ³D. G. Shchukin, E. Skorb, V. Belova, and H. Mohwald, *Adv. Mater.* **23**(17), 1922–1934 (2011).
- ⁴D. Niebuhr, *Wear* **263**, 295–300 (2007).
- ⁵M. Virot, T. Chave, S. I. Nikitenko, D. G. Shchukin, T. Zemb, and H. Mohwald, *J. Phys. Chem. C* **114**(30), 13083–13091 (2010).
- ⁶C. D. Ohl, M. Arora, R. Ikink, N. de Jong, M. Versluis, M. Delius, and D. Lohse, *Biophys. J.* **91**(11), 4285–4295 (2006).
- ⁷M. Eigen and L. Demeyer, *Z. Elektrochem.* **59**(10), 986–993 (1955).
- ⁸P. L. Geissler, C. Dellago, D. Chandler, J. Hutter, and M. Parrinello, *Science* **291**(5511), 2121–2124 (2001).
- ⁹D. D. Dlott, *Ann. Rev. Phys. Chem.* **50**, 251–278 (1999).
- ¹⁰A. Nakano, R. K. Kalia, K. Nomura, A. Sharma, P. Vashishta, F. Shimojo, A. C. T. van Duin, W. A. Goddard, R. Biswas, and D. Srivastava, *Comput. Mater. Sci.* **38**(4), 642–652 (2007).
- ¹¹K. Nomura, R. K. Kalia, A. Nakano, and P. Vashishta, *Comput. Phys. Commun.* **178**(2), 73–87 (2008).
- ¹²A. C. T. van Duin, S. Dasgupta, F. Lorant, and W. A. Goddard, *J. Phys. Chem. A* **105**(41), 9396–9409 (2001).
- ¹³D. W. Brenner, *Phys Status Solidi B* **217**(1), 23–40 (2000).
- ¹⁴T. Watanabe, *J. Comput. Electron.* **10**(1–2), 2–20 (2011).
- ¹⁵A. K. Rappe and W. A. Goddard, *J. Phys. Chem.* **95**(8), 3358–3363 (1991).
- ¹⁶C. D. Ohl and R. Ikink, *Phys. Rev. Lett.* **90**(21), 214502 (2003).
- ¹⁷A. Choubey, M. Vedadi, K. Nomura, R. K. Kalia, A. Nakano, and P. Vashishta, *Appl. Phys. Lett.* **98**, 023701 (2011).
- ¹⁸M. Vedadi, A. Choubey, K. Nomura, R. K. Kalia, A. Nakano, P. Vashishta, and A. C. T. van Duin, *Phys. Rev. Lett.* **105**(1), 014503 (2010).
- ¹⁹K. Nomura, R. K. Kalia, A. Nakano, and P. Vashishta, *Appl. Phys. Lett.* **91**(18), 183109 (2007).
- ²⁰K. Nomura, R. K. Kalia, A. Nakano, P. Vashishta, A. C. T. van Duin, and W. A. Goddard, *Phys. Rev. Lett.* **99**(14), 148303 (2007).
- ²¹V. Swamy, S. K. Saxena, B. Sundman, and J. Zhang, *J Geophys Res [Solid Earth Planets]* **99**(B6), 11787–11794, doi:10.1029/93JB02968 (1994).
- ²²K. Nomura, R. K. Kalia, A. Nakano, and P. Vashishta, *Appl. Phys. Lett.* **91**(18), 183109 (2007).
- ²³N. Agmon, *Chem. Phys. Lett.* **244**(5–6), 456–462 (1995).
- ²⁴F. Shimojo, S. Ohmura, R. K. Kalia, A. Nakano, and P. Vashishta, *Phys. Rev. Lett.* **104**(12), 126102 (2010).
- ²⁵G. Zundel and H. Metzger, *Z. Phys. Chem., Neue Folge* **58**(5–6), 225 (1968).